Homoclinic and Heteroclinic Bifurcations in rf SQUIDs

B. Bruhn and B. P. Koch

Sektion Physik/Elektronik, Ernst-Moritz-Arndt-Universität, Greifswald, DDR

Z. Naturforsch. **43 a**, 930–938 (1988); received September 1, 1988

The Melnikov method is used to discuss the parameter dependence of homoclinic and heteroclinic bifurcations for the rf SQUID system. Also the case of strong damping is treated. Because of the complicated potential the resulting integrals have to be evaluated numerically. For some selected parameter sets the theoretical predictions are compared with numerical solutions of the equation of motion. Very good agreement of both methods is found.

Key words: Nonlinear dynamics, Josephson effect, chaos, homoclinic and heteroclinic bifurcations

1. Introduction

It is well known that simple periodically forced nonlinear oscillators may show chaotic dynamics. Examples of such systems are the pendulum and the Duffing oscillator, on which a lot of numerical and experimental investigations have been published (see e.g. [1–6]).

An efficient analytical treatment for predicting chaotic motions is the Melnikov method [7–9]. The prerequisite for the application of this treatment is that the equations of motion can be written as the sum of an autonomous system with homoclinic (heteroclinic) orbits and a small time periodic perturbation. With the unperturbed solutions the so called Melnikov function has to be calculated, which is a measure of the distance (first order of the perturbation theory) between the stable and unstable manifolds of hyperbolic fixed points in the Poincaré map. If the Melnikov function has simple zeros, then there exist transverse homoclinic (heteroclinic) orbits.

In the homoclinic case, according to the Smale-Birkhoff homoclinic theorem [8], chaotic motions appear. Under additional conditions also in the heteroclinic case chaotic dynamics may exist [10].

Although the Melnikov method gives no possibility to distinguish between transient and permanent chaos there are many papers in which the Melnikov method is applied to simple periodically forced oscillators [11–16].

Mathematical difficulties arise in the calculation of the unperturbed homoclinic (heteroclinic) orbits and the resulting improper integral. Only in simple cases both operations can be performed analytically, and as a rule only numerical calculations are feasible.

In this paper we study a rf superconducting quantum interference device (SQUID) driven by an oscillating external flux. The equation of motion for the difference in the phase of the superconducting order parameter across the junction x is given by [17]

$$\ddot{x} + \frac{1}{\sqrt{\beta_c}}\,\dot{x} + \sin x + \frac{1}{\beta_L}\,x = \frac{2e}{\hbar\,\beta_L}\,\phi_{ex}\,. \tag{1.1}$$

The dot means differentiation with respect to the dimensionless time variable t,

$$t = \sqrt{\frac{2e\,I_c}{\hbar\,C}}\;\tau \quad (\tau = \text{time in seconds}),$$

and the periodic external flux is given by $\phi_{ex} = A \cdot \sin(\Omega t)$. β_c and β_L are the McCumber parameters which are connected with the resistance R, capacity C, inductance L and critical current I_c of the SQUID by

$$\beta_c = \frac{2e}{\hbar}\,I_c\,R^2\,C\,, \quad \beta_L = \frac{2e}{\hbar}\,LI_c\,,$$

where e and $\hbar$ are the elementary charge and Planck constant, respectively. Equation (1.1) can be regarded as describing a classical particle moving in the potential

$$V(x) = x^2/2\,\beta_L - \cos x \tag{1.2}$$

while it is being pertubed by frictional and periodic external forces. The case of a pure cosine potential, which corresponds to a single Josephson junction, has been investigated in several papers (for references see [6]).

Reprint requests to Dr. B. Bruhn, Sektion Physik-Elektronik, Universität Greifswald, Domstraße 10a, Greifswald 2200/DDR.

0932-0784 / 88 / 1100-0930 $ 01.30/0. – Please order a reprint rather than making your own copy.

Ritala and Salomaa [18, 19] and Fesser and Bishop [20] have numerically investigated the SQUID equation (1.1) and have found for different parameter values a lot of chaotic phenomena.

In a recent paper [21] the Melnikov method is applied to the rf-SQUID in the case of small damping and excitation. Using a polynomial approximation of the trigonometric function in $V(x)$, the analytical calculation of the Melnikov integrals becomes possible. The result is similar to the Melnikov function for the anti-Duffing oscillator [1].

In the present paper, for small damping and excitation the Melnikov method is applied without an approximation of the potential (1.2), and in a second part also the case of strong damping and small excitation is considered.

2. Calculation of the Bifurcation Conditions

The dimensionless equations of motion for the rf-SQUID (1.1) can be written in the form

$$\dot{x} = y,$$
$$\dot{y} = -\sin x - c\,x + \varepsilon(a \cdot \sin \Omega t - b\,y), \tag{2.1}$$

where

$$c \equiv 1/\beta_L, \quad \varepsilon \cdot b \equiv 1/\sqrt{\beta_c}, \quad \varepsilon\, a \equiv 2e\,A/\hbar\,\beta_L .$$

Because the Melnikov method is based on perturbation theory, we have introduced a small parameter ε ($0 \leqq \varepsilon \ll 1$) into the equations of motion.

The corresponding unperturbed system ($\varepsilon = 0$)

$$\dot{x}_0 = y_0, \quad \dot{y}_0 = -\sin x_0 - c\,x_0 \tag{2.2}$$

has the energy as a first integral

$$H = \tfrac{1}{2}\,y_0^2 + \tfrac{1}{2}\,c\,x_0^2 - \cos x_0 , \tag{2.3}$$

where the quadratic potential term yields the effect of confining the motion in x-space. Depending upon the potential parameter c, there may exist a great variety of separatrix solutions and associated hyperbolic fixed points in the phase space of (2.2). Figures 1 and 2 show these separatrix solutions for two selected values of the parameter c. One obtains the hyperbolic fixed points $P = (\bar{x}_0, 0)$ from the conditions

$$\sin \bar{x}_0 + c\,\bar{x}_0 = 0, \quad c + \cos \bar{x}_0 < 0, \tag{2.4}$$

and the energy E of the separatrices by the solutions of (2.4) and

$$E = \tfrac{1}{2}\,c\,\bar{x}_0^2 - \cos \bar{x}_0 . \tag{2.5}$$

The Melnikov function may be written in the form [9]

$$M(t_0) = \int_{-\infty}^{\infty} \hat{X}_s\, H \, \mathrm{d}t , \tag{2.6}$$

where $\hat{X}_s$ is the vector field of the perturbation

$$\hat{X}_s = (a \cdot \sin \Omega t - b\,y_0)\, \partial/\partial y_0$$

which acts on the first integral (2.3). For the practical analysis of the Melnikov integral one needs the unperturbed separatrix solutions as a function of t and the initial time t_0. This solution can be obtained analytically only in very few cases, so that a numerical calculation of (2.6) must be used. Such numerical implementation of the Melnikov method has been proposed by Ling and Bao in a recent paper [22].

However, we use a different approach which also works in some cases where the function $t(t_0, y_0)$ is known but the inversion is not possible. The basic concept is to substitute the space variable x_0 for the integration variable t in (2.6).

Because our unperturbed system (2.2) contains both heteroclinic and homoclinic orbits, the different cases are treated separately. At first we consider the case of an upper heteroclinic solution. From (2.2), (2.3) one obtains

$$t = t_0 + \int_0^{x_0} \frac{\mathrm{d}z}{\sqrt{2E - c\,z^2 + 2\cos z}} . \tag{2.7}$$

Moreover, with (2.6) and (2.7),

$$\begin{aligned} M(t_0) &= \int_{-\infty}^{\infty} (a\,y_0 \sin \Omega t - b\,y_0^2)\,\mathrm{d}t \\ &= -2b \int_0^{\bar{x}_0} \sqrt{2E - c\,z^2 + 2\cos z}\,\mathrm{d}z \\ &\quad + a \int_{-\bar{x}_0}^{0} \sin \Omega \left(t_0 + \int_0^{x_0} \frac{\mathrm{d}z}{\sqrt{2E - c\,z^2 + 2\cos z}} \right) \mathrm{d}x_0 \\ &\quad + a \int_0^{\bar{x}_0} \sin \Omega \left(t_0 + \int_0^{x_0} \frac{\mathrm{d}z}{\sqrt{2E - c\,z^2 + 2\cos z}} \right) \mathrm{d}x_0 , \end{aligned}$$

where $\bar{x}_0$ is the coordinate of the hyperbolic fixed point in the right phase space region and E the associated energy of the heteroclinic orbit. Using some elementary properties of the sine function and some

symmetries, the Melnikov function finally reads

$$M(t_0) = -2b \cdot F(c) + 2a \cdot G(c, \Omega) \sin \Omega t_0 , \qquad (2.8)$$

$$F(c) \equiv \int_0^{\bar{x}_0} \sqrt{2E - c z^2 + 2 \cos z}\, \mathrm{d}z ,$$

$$G(c, \Omega) \equiv \int_0^{\bar{x}_0} \cos\left(\Omega \cdot \int_0^{x_0} \frac{\mathrm{d}z}{\sqrt{2E - c z^2 + 2 \cos z}} \right) \mathrm{d}x_0 .$$

Note that also the position of the fixed point $\bar{x}_0$ and the energy of the homoclinic orbit E depend on the potential parameter c.

For the homoclinic case we need an additional information on the turning points $(\bar{x}_0, 0)$ of the unperturbed system. These points are the solutions of the transcendent equation

$$c \bar{x}_0^2 - 2 \cos \bar{x}_0 = 2E , \qquad (2.9)$$

which are not the fixed point solutions. E denotes the energy of the corresponding homoclinic orbit. Also in this case the integration variable of the Melnikov integral is changed to x_0 and the fixed points and turning points are the limits. A short calculation yields

$$M(t_0) = -2b \cdot \tilde{F}(c) - 2a \cdot \tilde{G}(c, \Omega) \cos \Omega t_0 , \qquad (2.10)$$

where

$$\tilde{F}(c) \equiv \int_{\bar{x}_0}^{\bar{x}_0} \sqrt{2E - c z^2 + 2 \cos z}\, \mathrm{d}z ,$$

$$\tilde{G}(c, \Omega) \equiv \int_{\bar{x}_0}^{\bar{x}_0} \sin\left(\Omega \cdot \int_{\bar{x}_0}^{x_0} \frac{\mathrm{d}z}{\sqrt{2E - c z^2 + 2 \cos z}} \right) \mathrm{d}x_0 .$$

The existence of Smale's horseshoes in the dynamics is related to the zeros of the Melnikov integral as a function of t_0. Equations (2.8) and (2.10) indicate that simple zeros of $M(t_0)$ may exist. The boundary of the horseshoe region in the parameter space results from the bifurcation conditions. These conditions are given by:

(i) heteroclinic case: $a/b = |F(c)/G(c, \Omega)|$, (2.11)

(ii) homoclinic case: $a/b = |\tilde{F}(c)/\tilde{G}(c, \Omega)|$. (2.12)

For larger values of the ratio of excitation and damping than in (2.11) and (2.12) we find transverse intersections of stable and unstable manifolds of the hyperbolic fixed points of the associated Poincaré map. Therefore chaotic motions can be observed. We cannot, however, predict whether the motion becomes transiently or permanently chaotic. But the numerical simulation of (2.1) indicates that near the bifurcation values (2.11) and (2.12) transient chaos occurs for small ε.

3. The Case of Strong Damping

The SQUID equation (1.1) cannot be written in the form of (2.1) for small values of the parameter β_c. In this case we have

$$\dot{x} = y, \quad \dot{y} = -\sin x - c x - b y + \varepsilon \cdot \sin \Omega t , \qquad (3.1)$$

where

$$c \equiv 1/\beta_L , \quad b \equiv 1/\sqrt{\beta_c} \quad \text{and} \quad \varepsilon \equiv 2e A/h \beta_L .$$

The associated unperturbed system

$$\dot{x} = y, \quad \dot{y} = -\sin x - c x - b y \qquad (3.2)$$

contains the damping b, so that the energy is no longer a conserved quantity. In this section the index 0, which indicates the unperturbed system, is dropped. From (3.2) follows that the degradation of energy along an arbitrary orbit is always positive, i.e.

$$\frac{\mathrm{d}H}{\mathrm{d}t} = \frac{\mathrm{d}}{\mathrm{d}t}\left(\tfrac{1}{2} y^2 + \tfrac{1}{2} c x^2 - \cos x\right) = -b y^2 < 0 . \qquad (3.3)$$

The system (3.2) is a multistable system, and therefore each solution tends to one of the fixed points as $t \to +\infty$. These points are given by

$$c \bar{x} + \sin \bar{x} = 0, \quad \bar{y} = 0 ,$$

The linearization of the vector field at an equilibrium yields

$$\lambda_{\pm} = -b/2 \pm \sqrt{b^2/4 - c - \cos \bar{x}} , \qquad (3.4)$$

i.e. for $c + \cos \bar{x} < 0$ the fixed points are saddle points and for $c + \cos \bar{x} > 0$ spiral points ($b^2 < 4(c + \cos \bar{x})$) or nodal points ($b^2 > 4(c + \cos \bar{x})$).

The most interesting case is given by sufficiently small parameters c so that at least 4 hyperbolic fixed points exist. Then the following proposition is valid.

Proposition:

(i) For a fixed value of c, there exists an infinite sequence $\{x_k^H(t), y_k^H(t)\}$ of heteroclinic orbits of (3.2) depending upon a discrete set of damping parameters b_k, $k = 1, 2, \ldots$.

(ii) The value $b = +0$ is a limit element, i.e. in each small but finite interval $0 \leqq b_k < b_\varepsilon$ one finds an infinite subset of the sequence.

(iii) There is an upper bound b_M, so that for $b > b_M$ there is no heteroclinic orbit.

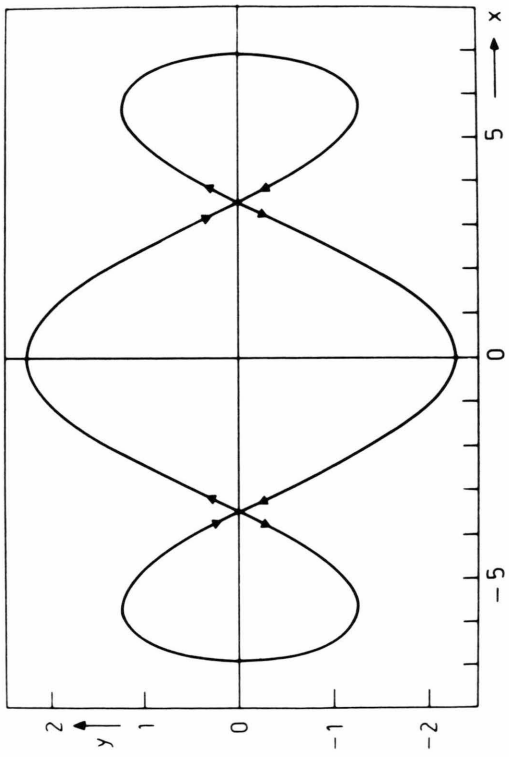

Fig. 1. Unperturbed manifolds of (2.2). $c = 0.1$, $E = 1.5489$.

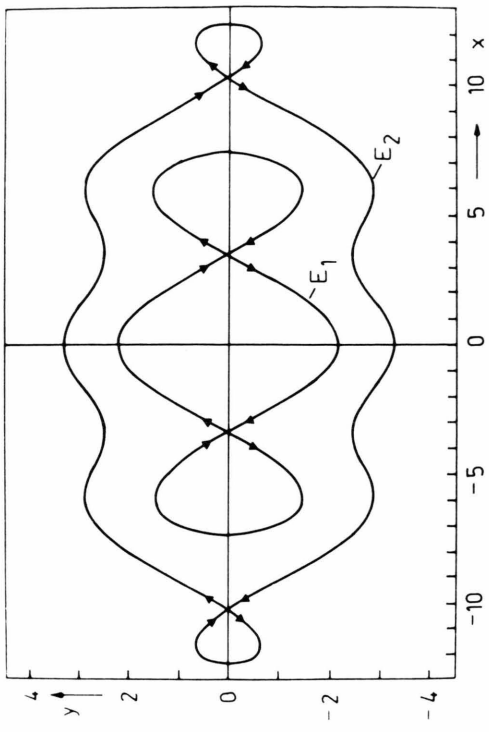

Fig. 2. Unperturbed manifolds of (2.2). $c = 0.07$, $E_1 = 1.3715$, $E_2 = 4.356$.

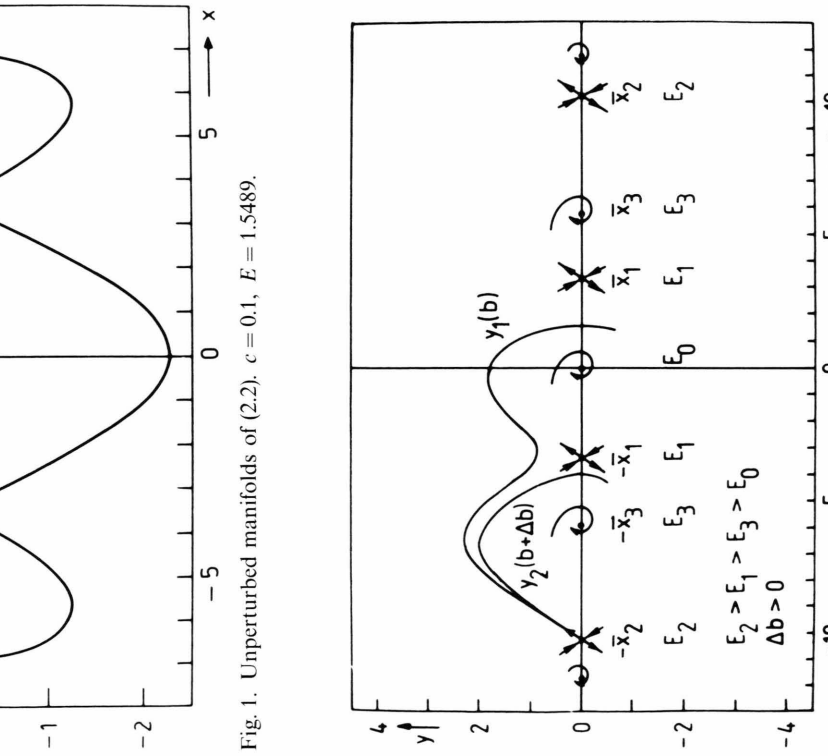

Fig. 3. Fixed points and the unstable manifold of one outer saddle for $c = 0.07$ and two different b values (see (3.2)).

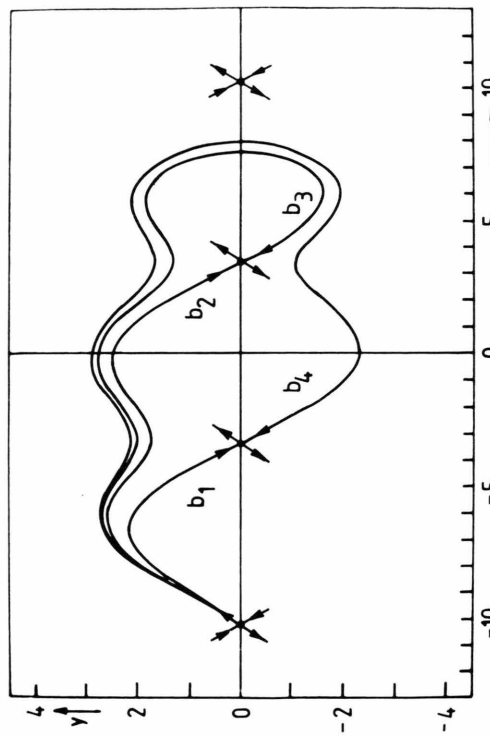

Fig. 4. Heteroclinic orbits of (3.2) with $N = 0$, $c = 0.07$. $b_1 = 0.328913\ldots$, $b_2 = 0.12172\ldots$, $b_3 = 0.07681\ldots$, $b_4 = 0.05389\ldots$.

Proof:

Without any restriction we consider the case of 4 saddle points only (the first nontrivial case). Then the heteroclinic orbit for $b \neq 0$ must be a saddle-saddle connection from an outer to an inner hyperbolic fixed point ($dE/dt < 0$).

Figure 3 shows a generic situation for two initial conditions which are located on the unstable manifold (for $y(t \to -\infty) > 0$) of the outer hyperbolic fixed point in the left part of the phase plane. Here we have assumed that $b^2 < 4(c + \cos \bar{x})$, so that the stable equilibrium points are spiral points. By a suitable choice of Δb, the final states are neighbouring spiral points, e.g. $-\bar{x}_3$ and 0.

In a first step we compare the degradation of energy along y_1 with the degradation along y_2 for the interval $[-\bar{x}_2, -\bar{x}_1]$:

$$\Delta E|_{y_1} = b \int_{-\bar{x}_2}^{-\bar{x}_1} y_1 \, dx < (E_2 - E_1). \tag{3.5}$$

Instead of the full solution y_2 we use

$$y_2^+(x) = \begin{cases} y_2(x) & \text{for} \quad -\bar{x}_2 \leqq x \leqq \eta, \\ 0 & \text{for} \quad \eta < x \leqq -\bar{x}_1, \end{cases}$$

where η is the first turning point of y_2. Then

$$\Delta E|_{y_2^+} = (b + \Delta b) \int_{-\bar{x}_2}^{-\bar{x}_1} y_2^+ \, dx > (E_2 - E_1), \tag{3.6}$$

Using the continuous dependence solutions on parameters, we obtain

$$\Delta b \to 0: \quad y_2 \to y_1 \quad \text{or} \quad y_2^+ \to y_1 \quad \text{in} \quad [-\bar{x}_2, -\bar{x}_1].$$

Also the degradation of energy must proceed continuously from (3.6) to (3.5) with $\Delta b \to 0$. But because of the two inequalities there must be a value b' with $b < b' < b + \Delta b$ and a corresponding solution $y'(t)$ so that

$$E_2 - E_1 \overset{!}{=} b' \int_{-\bar{x}_2}^{-\bar{x}_1} y' \, dx .$$

The uniqueness theorem secures that y' is the saddle-saddle connection from $-\bar{x}_2$ to $-\bar{x}_1$. Actually, we have used the property that the heteroclinic orbit is a basin boundary between two stable attractors.

In the second step we assume that b is sufficiently small, so that the first turning point comes near the outer hyperbolic fixed point $\bar{x}_2$. Then the phase space trajectory rotates around the inner fixed point region with a decreasing amplitude, and after a certain number of rotations N, it tends to one of the stable equilibrium points. Using the arguments of the first step, one can see that to each number of rotations N at least one heteroclinic orbit is associated. More precisely, in the case of 4 hyperbolic fixed points there are 8 different heteroclinic orbits to each N (using the full symmetry of (3.2)).

The degradation of energy for the j-th rotation can be obtained by perturbation theory because b is sufficiently small:

$$\Delta E_j \approx b \int_{P_j} (y_{0j})^2 \, dt = b \, k_j ,$$

where y_{0j} is a solution of (2.2) with period P_j and the energy of this solution is in the interval $E_2 > E > E_1$. The whole degradation of energy in the rotation stage is

$$\Delta E = \sum_{j=1}^{N} \Delta E_j = b \sum_{j=1}^{N} k_j \approx E_2 - E_1 . \tag{3.7}$$

From the definition of the k_j follows that these constants do not depend upon b and that there is an upper and a lower bound

$$k_j < \mu_1 = 2 \int_{-\infty}^{\infty} (y_{\text{het}}^{\text{A}})^2 \, dt ,$$

$$k_j > \mu_2 = 2 \int_{-\infty}^{\infty} (y_{\text{het}}^{\text{I}})^2 \, dt + 2 \int_{-\infty}^{0} (y_{\text{hom}}^{\text{I}})^2 \, dt ,$$

where $y_{\text{het}}^{\text{A}}$ is the outer heteroclinic, $y_{\text{het}}^{\text{I}}$ the inner heteroclinic and $y_{\text{hom}}^{\text{I}}$ the inner homoclinic solution of (2.2) (cf. also Fig. 2).

With the estimation

$$k_j \approx \tfrac{1}{2}(\mu_1 + \mu_2) \equiv \mu$$

one finds (3.7) in the following form

$$E_2 - E_1 \approx \mu \, b N \;\to\; N \sim 1/b , \tag{3.8}$$

and because to each N at least one heteroclinic orbit is associated the statements (i) and (ii) follow directly from (3.8). The existence of an upper bound b_{M} is obvious from Fig. 3, e.g. an upper bound is given by $b = 2\sqrt{c+1}$, where a saddle-node connection exists. This completes the proof.

Figure 4 shows the first 4 heteroclinic orbits in the case $N = 0$ associated with the outer hyperbolic fixed point in the left part of the phase plane for $c = 0.07$ and four different b values. We have determined the values b_k by an iterative method using the basin boundary property of the heteroclinic orbit.

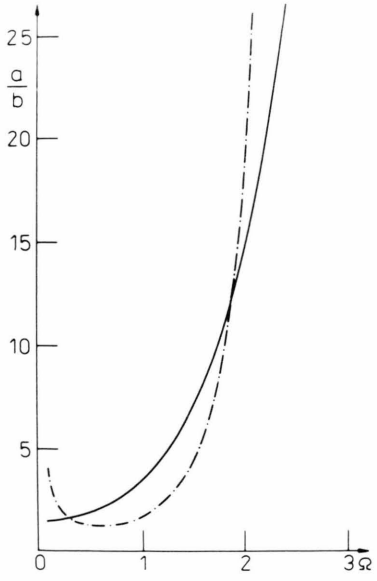

Fig. 5. Bifurcation functions for the homoclinic (dash-dotted curve) and heteroclinic (solid curve) cases. $c = 0.1$, $E = 1.5489$.

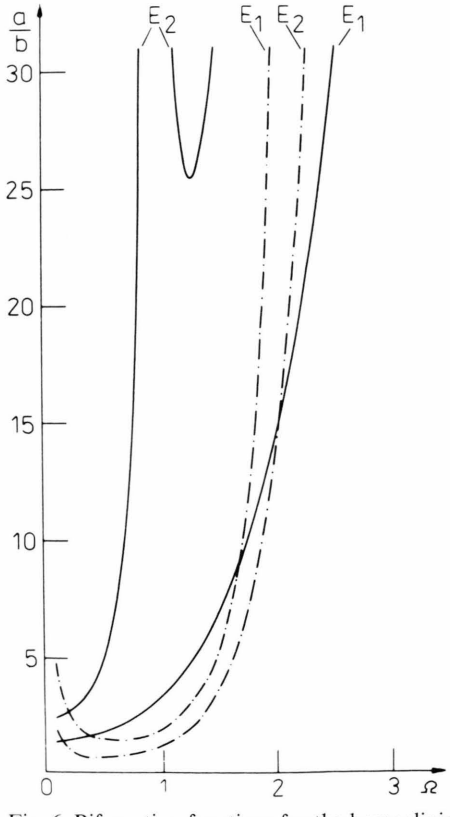

Fig. 6. Bifurcation functions for the homoclinic (dash-dotted curves) and heteroclinic (solid curves) cases. $c = 0.07$, $E_1 = 1.3715$, $E_2 = 4.356$.

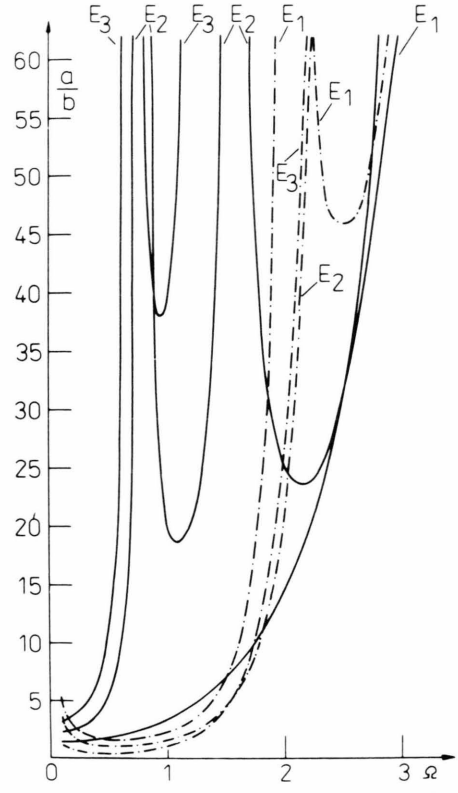

Fig. 7. Bifurcation functions for the homoclinic (dash-dotted curves) and heteroclinic (solid curves) cases. $c = 0.05$, $E_1 = 1.259$, $E_2 = 3.340$, $E_3 = 7.519$.

Consider now the perturbed system (3.1). Actually, this is a special case in a class of highly damped system [23]. Instead of (2.6) the following modified Melnikov function must be considered here:

$$M(t_0) = \int_{-\infty}^{\infty} y_k^{\mathrm{H}}(t) \cdot \sin \Omega(t + t_0) \cdot \exp(b_k t)\, \mathrm{d}t, \qquad (3.9)$$

where y_k^{H} is one of the unpertubed heteroclinic orbits of (3.2). The exponential factor is necessary because the divergence of the phase velocity of (3.2) is not zero. (3.9) can also be represented in the form

$$M(t_0) = A(\Omega, b_k, c) \sin \Omega t_0 + B(\Omega, b_k, c) \cos \Omega t_0,$$

where

$$A \equiv \int_{-\infty}^{\infty} y_k^{\mathrm{H}}(t, b_k, c) \cdot \cos \Omega t \cdot \exp(b_k t)\, \mathrm{d}t,$$

$$B \equiv \int_{-\infty}^{\infty} y_k^{\mathrm{H}}(t, b_k, c) \cdot \sin \Omega t \cdot \exp(b_k t)\, \mathrm{d}t. \qquad (3.10)$$

As $t \to \pm\infty$, the function $y_k^{\mathrm{H}} \cdot \exp(b_k t)$ tends exponentially to zero, which follows from (3.4). Thus the inte-

grals A, B are finite and the Melnikov function is well defined.

Further on, using the arguments in [23, 24], A and B do not vanish except on a discrete set of frequencies Ω. This suffices to establish the existence of simple zeros and thus of transverse heteroclinic points for all small ε.

As a consequence of the structural stability of heteroclinic intersections there is around each critical value of b_k a small but finite interval so that one finds transverse intersections for all b values within this interval. We suppose that for sufficiently small values of b there is an overlapping of these intervals.

However, from the phase space topology follows that we can not find a heteroclinic cycle and thus no horseshoe construction is possible [8], i.e. the resulting dynamics is nonchaotic. The existence of transverse heteroclinic points implies a complicated structure of the basin boundaries of the different nonchaotic attractors. This follows from the fact that the stable manifolds of the inner hyperbolic fixed points oscillate around the instable manifolds of the outer saddle points and accumulate on the stable manifold of the outer saddles. The intersection of a typical line with the closure of the stable manifold produces an infinite sequence of open intervals which alternately correspond to different attractors. The infinite set of crossing points is not a Cantor set, therefore the basin boundary is not fractal. Nevertheless, near the stable manifolds of the outer saddles one observes a delicate final state sensitivity.

4. Discussion and Numerical Experiments

The numerical analysis is divided into two parts. The first part contains the numerical calculation of the bifurcation conditions (2.11/12), and in the second part the predictions of the Melnikov method are checked for some selected parameter values.

The fixed points and the turning points of the unperturbed system are calculated from (2.4) and (2.9) with the aid of a Newton method, and we have used a standard programme for the definite integrals in $F(c)$, $\tilde{F}(c)$, $G(c, \Omega)$ and $\tilde{G}(c, \Omega)$. Note that the integrand of $G(c, \Omega)$ and $\tilde{G}(c, \Omega)$ contains a singularity at the fixed points. This singularity results from the original Melnikov integral as an improper integral. Actually, we have calculated an integral with limits of integration near these critical points ($x_0 \to x_0 + \mu$, $\mu \to 0$), and as an error control the value of μ has been varied.

Figure 5–7 show the bifurcation functions for three different values of the potential parameter c. A decrease of this parameter leads to a more complicated separatrix structure of the unperturbed system. Especially Fig. 7 shows a complicated bifurcation structure. Near the calculated curves there are further bifurcations, e.g. saddle-node and period doubling bifurcations.

For the same parameter $c = 0.05$ Ritala and Salomaa [19] have obtained, by numerical integration of (1.1), existence regions for different subharmonic and permanent chaotic solutions. Also these regimes display an extremely delicate structure.

The global behaviour of the bifurcation functions (Figs. 5–7) indicates that there are regions in the parameter space where there are homoclinic and no heteroclinic intersections, and vice versa. This is a typical effect in complicated systems [15]. Moreover, the inner manifolds intersect in other regions of the parameter space than the outer ones. For selected values of the frequency the zeros of $G(c, \Omega)$, $\tilde{G}(c, \Omega)$ produce poles of the functions (2.11) and (2.12). Possibly, additional contributions from higher order Melnikov functions [25] remove the poles from the bifurcation functions.

In order to check some of these predictions, we have numerically calculated, for the Poincaré map of (2.1), parts of the stable and unstable manifolds coming from the hyperpolic fixed points. The parameter values corresponding to Fig. 8 are used to produce homoclinic but not heteroclinic intersections (cf. Figure 5). At larger values of the ratio a/b and the same Ω one finds both homoclinic and heteroclinic intersections. Figure 9 illustrates this situation for $a = 3.0$ and $b = 1.0$.

Figure 10 shows a configuration of 4 hyperbolic fixed points arising from a smaller potential parameter c (for the corresponding unperturbed problem cf. Figure 2). Especially, such parameters are chosen that the inner and outer manifolds produce homoclinic intersections; moreover, the outer manifolds do not show heteroclinic intersections. For the inner manifolds the values are slightly above the heteroclinic bifurcation situation (bifurcation value: $a/b \approx 2.6$). The manifolds form a complicated network structure, and we have shown only a small part of them.

In order to check the predictions of Sect. 3, we have numerically calculated, for the Poincaré map of (3.1), parts of the stable and unstable manifolds. Figure 11

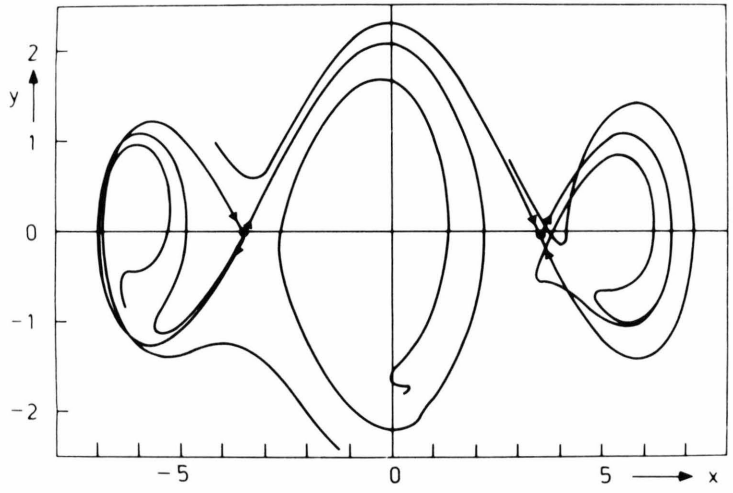

Fig. 8. Parts of the stable and unstable manifolds of the hyperbolic fixed points corresponding to the Poincaré map of (2.1). Parameter set: $c = 0{,}1$, $\varepsilon = 0.1$, $\Omega = 0.8$, $a = 1.0$, $b = 0.5$.

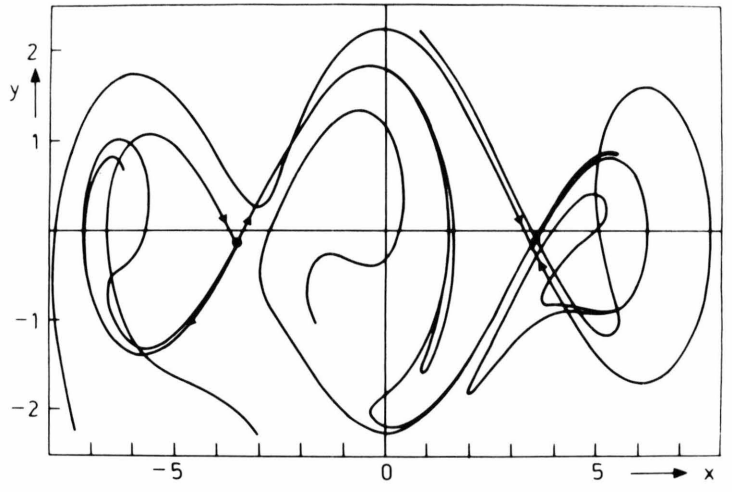

Fig. 9. Parts of the stable and unstable manifolds of the hyperbolic fixed points corresponding to the Poincaré map of (2.1). Parameter set: $c = 0.1$, $\varepsilon = 0.1$, $\Omega = 0.8$, $a = 3.0$, $b = 1.0$.

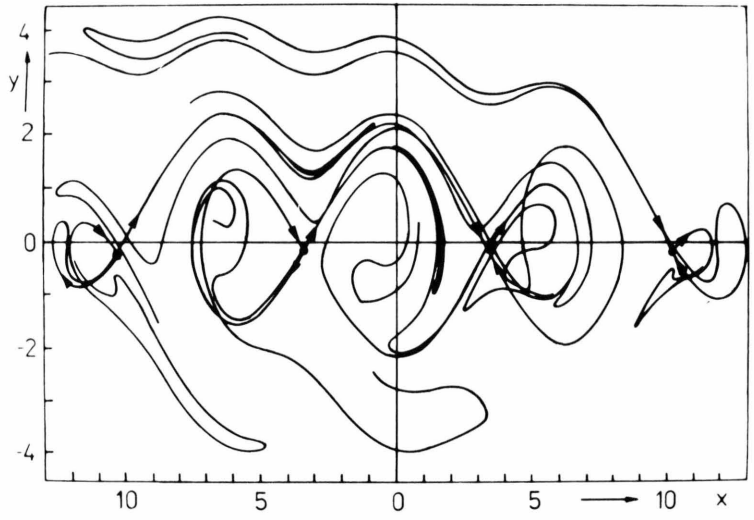

Fig. 10. Parts of the stable and unstable manifolds of the hyperbolic fixed points corresponding to the Poincaré map of (2.1). Parameter set: $c = 0.07$, $\varepsilon = 0.1$, $\Omega = 0.8$, $a = 2.65$, $b = 1.0$.

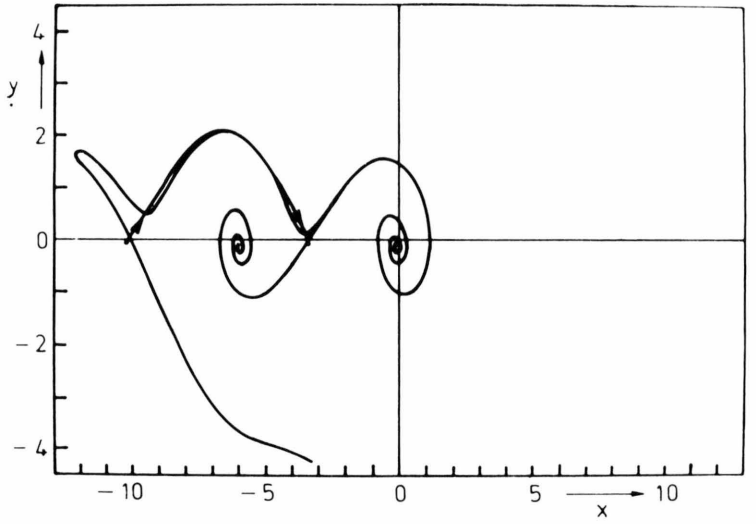

Fig. 11. Parts of the stable and unstable manifolds of the hyperbolic fixed points corresponding to the Poincaré map of (3.1). Parameter set: $c = 0.07$, $\varepsilon = 0.1$, $\Omega = 1.2$, $b = 0.3289133$.

shows the result, where the parameter value of $b = 0.328913\ldots$ corresponds to a heteroclinic orbit of (3.2) from the outer to the inner hyperbolic fixed point in the left part of the phase plane. Clearly visible is the predicted crossing of the manifolds for the perturbed system (3.1). Especially the unstable manifold spirals around the sinks which correspond to $(0, 0)$ and $(-\bar{x}_3, 0)$ in the unperturbed case.

The final state sensitivity can be demonstrated in the following numerical experiment. Applying a fourth order Runge-Kutta method with the same parameters as in Fig. 11 and fixed initial conditions ($x = -10.224798399$, $y = -0.05606$), the SQUID system (3.1) is integrated using two different step sizes Δt. The final state is the left sink for $\Delta t = 0.032$ and the right sink (cf. Fig. 11) for $\Delta t = 0.033$. This numerical effect is caused by the complicated boundary structure.

For the SQUID system the case $b \ll 1$ is very interesting, because on the one hand one finds heteroclinic and homoclinic bifurcations (cf. Sect. 2), which lead to chaotic behaviour and to a fractal basin boundary structure [26]. On the other hand there are the heteroclinic intersections discussed in Section 3. We assume that the discussed transient phenomena should be observable also in real SQUID experiments.

Our discussion shows that the Melnikov method can successfully be applied to systems with complicated potentials, for which an analytic calculation of the associated integrals is not possible. The expense in numerical calculation is relatively low, therefore we recommend this numerical implementation of the Melnikov method, to find out parameter regions of complicated behaviour.

Acknowledgements

The authors would like to thank T. Meyer for his assistance in the solution of various numerical problems.

[1] P. J. Holmes, Philos. Trans. Roy Soc. London **A 292,** 419 (1979).
[2] F. C. Moon and P. J. Holmes, J. Sound Vib. **65,** 285 (1979).
[3] B. A. Huberman and J. P. Crutchfield, Phys. Rev. Lett. **43,** 419 (1979).
[4] Y. Ueda, Ann. N.Y. Acad. Sci. **357,** 427 (1980).
[5] R. W. Leven, B. Pompe, C. Wilke, and B. P. Koch, Physica **16 D,** 371 (1985).
[6] R. L. Kautz and J. C. Macfarlane, Phys. Rev. **A 32,** 498 (1986).
[7] V. K. Melnikov, Tr. Moskovsk. Ob-va **12,** 3 (1963).
[8] J. Guckenheimer and P. J. Holmes, Nonlinear Oscillations, Dynamical Systems, and Bifurcations of Vector Fields. Appl. Math. Sciences **42,** Springer, New York 1983.
[9] B. Bruhn and R. W. Leven, Physica Scripta **32,** 486 (1985).
[10] P. J. Holmes, Lect. Notes Math. **898,** 164 (1981).
[11] P. J. Holmes, SIAM J. Appl. Math. **38,** 65 (1980).
[12] B. P. Koch and R. W. Leven, Physica **16 D,** 1 (1985).
[13] F. M. A. Salam and S. S. Sastry, IEEE Trans. Circuits Syst. CAS-**32,** 784 (1985).
[14] K. Hockett and P. J. Holmes, Ergod. Th. Dynam. Syst. **6,** 205 (1986).
[15] B. P. Koch, Phys. Lett. **A 117,** 302 (1986).
[16] B. P. Koch and B. Bruhn, J. Phys. France **49,** 35 (1988).
[17] K. K. Licharev, Vvedenie v dinamiku dshozevsonovskich perechodov. Nauka, Moskva 1985.
[18] R. K. Ritala and M. M. Salomaa, J. Phys. C: Solid State Phys. **16,** L 477 (1983).
[19] R. K. Ritala and M. M. Salomaa, Phys. Rev. **B 29,** 6143 (1984).
[20] K. Fesser, A. R. Bishop, and P. Kumar, Appl. Phys. Lett. **43,** 123 (1983).
[21] W. C. Schieve, A. R. Bulsara, and E. W. Jacobs, Phys. Rev. **A 37,** 3541 (1988).
[22] F. H. Ling and G. W. Bao, Phys. Lett. **A 122,** 413 (1987).
[23] F. M. A. Salam, SIAM J. Appl. Math. **47,** 232 (1987).
[24] S. Schecter, SIAM J. Math. Anal. **18,** 1699 (1987).
[25] A. Aubanel, Lect. Notes Phys. **179,** 266 (1983).
[26] C. Grebogi, E. Ott, and J. A. Yorke, Physica **24 D,** 243 (1987).